Korean J. Chem. Eng., 38(6), 1139-1148 (2021)
DOI: 10.1007/s11814-021-0748-x

pISSN: 0256-1115
eISSN: 1975-7220

Direct synthesis of hydrogen peroxide over palladium catalysts supported on glucose-derived amorphous carbons

Hang Thi Thuy Vu, Viet Le Nam Vo, and Young-Min Chung†

Department of Nano & Chemical Engineering, Kunsan National University,
558 Daehak-ro, Kunsan, Jeollabuk-do 54150, Korea
(*Received 20 October 2020 • Revised 10 December 2020 • Accepted 26 January 2021*)

Abstract−Untreated and sulfonated biomass-derived amorphous carbons were prepared by the pyrolysis of D-glucose at different temperatures, followed by sulfonation. Not only the surface functional group concentration but also the structure of polyaromatic carbon sheets was significantly affected by the carbonization temperature and sulfonation. More importantly, the carbonization temperature played a crucial role in determining the size of Pd nanoparticles (NPs) on glucose-derived carbons (GCx) and thereby affected the catalytic performance of Pd/GCx for the direct synthesis of hydrogen peroxide (DSHP). The volcano-shaped dependency between the Pd NP size and the carbonization temperature of GCx agrees well with the reverse relationship between the Pd NP size and the catalytic activity of Pd/GCx. The flexible polyaromatic carbon sheet structure of the GCx was beneficial in increasing the sulfonic acid group content on the carbon surface and, therefore, H_2O_2 selectivity was improved in the presence of the Pd/S-GC2 catalyst (Pd supported on the sulfonated glucose-derived carbon pyrolyzed at 723 K). However, both H_2 conversion and H_2O_2 productivity decreased over the same catalyst, possibly due to the decreased number of active sites on the clustered or single-site Pd. Reducing the catalyst resulted in a decrease in H_2O_2 selectivity by significantly lowering the Pd^{2+}/Pd^0 ratio and increasing the Pd NP size. These results clearly demonstrate that fine control of the physicochemical properties of the active metal and GCx support and their synergistic combination is essential to realize an efficient Pd catalyst supported on GCx for the DSHP reaction.

Keywords: Direct Synthesis, Hydrogen Peroxide, Pd/C, Carbonization, Sulfonation

INTRODUCTION

Direct synthesis of hydrogen peroxide (H_2O_2; DSHP) from H_2 and O_2 is considered one of the most promising alternatives to the currently prevailing anthraquinone oxidation (AO) process. The AO process requires multiple energy-intensive reaction and separation steps along with an excessive use of toxic compounds [1,2]. By contrast, DSHP follows a straightforward reaction route along with high atom utilization efficiency, thus making the reaction attractive from environmental and economic viewpoints [3-6]. Moreover, considering safety in terms of the transportation of highly concentrated H_2O_2, the more flexible production scale of the DSHP process is clearly beneficial, e.g., on-site production of H_2O_2 [7].

However, commercial implementation of the DSHP process has not yet been realized despite its promising prospects. The reason is the low H_2O_2 yield involved with the intrinsic thermodynamic and safety issues of the reaction [6]. Regarding intrinsic thermodynamics, it is difficult to suppress the thermodynamically more favorable side-reactions promoted by the same active site, as described in Scheme 1. The safety issues of the reaction are closely related to the limitation of H_2 concentration below a threshold level to prevent any potential H_2/O_2 mixture explosion. Thus, numerous studies have been conducted in the past to improve the H_2O_2 yield, which is hampered by the inherent challenges of the DSHP reaction [8-11].

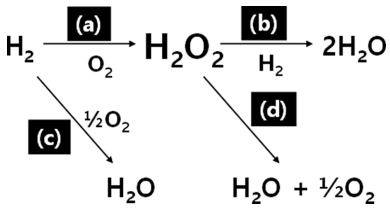

Scheme 1. Reaction pathways related to the DSHP from H_2 and O_2: (a) H_2O_2 synthesis, (b) H_2O_2 hydrogenation, (c) direct H_2 oxidation, and (d) H_2O_2 decomposition.

Among the various catalysts tested, palladium (Pd) catalysts supported on carbon materials (generally denoted as Pd/C) have been widely used in the DSHP reaction by virtue of the benign aspects of carbon-based supports, *i.e.*, competitive price, availability, and robustness in acidic or basic media [12,13]. In particular, the easy recovery of expensive Pd simply by burning off the carbon is clearly another advantage of the use of carbon-based supports from an economic viewpoint [13]. However, preparing an efficient Pd/C catalyst for the DSHP reaction is difficult. Despite the promising potential of carbon-based supports, conventional Pd/C catalysts result in low H_2O_2 yields, particularly in the absence of caustic acids and halide compounds. The heterogeneous and irregular carbon

†To whom correspondence should be addressed.
E-mail: ymchung@kunsan.ac.kr

Table 1. Changes in the functional group concentration on GCx depending on the carbonization temperature and sulfonation

Carbon support	Glucose carbonization temperature (K)	Functional group concentration (mmol/g)				
		Total	-COOH	-RCOR	-OH	$-SO_3H$
GC1	573	0.106	0.005	0.023	0.078	-
GC2	723	0.083	0.001	0.020	0.062	-
S-GC2		2.030	0.109	0.001	0.120	1.80
GC3	773	0.048	-	0.042	0.006	-
GC4	873	0.041	-	0.041	-	-
GC5	973	0.040	-	0.040	-	-

surface is not fully understood, and it becomes increasingly complex when the carbon surface is modified and/or an active metal is supported on the surface. This situation implies that the sophisticated control of the surface properties of the carbon support as well as the properties of the active metal is important in designing Pd/C catalysts for the DSHP reaction.

In this context, diverse strategies have been envisaged, focusing on the variation of the geometric and electronic properties of both active metals and carbon supports [14-20]. A range of potential Pd/C catalysts prepared by selective adsorption [21], sequential ligand exchange [22], and non-noble-metal sacrificial methods [23] have also been studied. These studies indicated that the formation of small Pd nanoparticles (NPs) within the sub-nanometer domain, either by the selective adsorption of cationic Pd precursors on the negatively charged carbon surface or by regulating the Pd NP growth during reduction, is of prime importance in improving the catalytic performance of Pd/C. Moreover, the functional groups present on the carbon surface and the additional heat treatment after Pd impregnation greatly affect the geometric and electronic nature of Pd and consequently the catalytic activity of Pd/C [24,25].

In this study, we prepared a range of Pd catalysts supported on glucose-derived amorphous carbons by carbonization at different temperatures and/or sulfonation. Subsequently, the catalytic performance of the resulting Pd/C for the DSHP reaction was investigated. The results revealed that the modified surface properties of the glucose-derived carbon (GCx) by heat treatments and/or sulfonation played crucial roles in determining the catalytic performance of Pd/C for the DSHP reaction.

EXPERIMENTAL

1. Chemicals

D-Glucose and ferroin indicator ($[Fe(C_{12}C_8N_2)_3]SO_4$, 0.1 wt% in H_2O) were obtained from Sigma-Aldrich. Tetraamminepalladium(II) nitrate solution ($Pd(NH_3)_4(NO_3)_2$, 5 wt% Pd) and sulfuric acid (H_2SO_4, 98%) were purchased from Strem and Daejung Chemicals (Korea), respectively. A 0.1 N cerium(IV) sulfate solution ($Ce(SO_4)_2$) was obtained from Merck Millipore. Hydrogen peroxide (H_2O_2, 34.5 wt%), sodium bicarbonate ($NaHCO_3$, 99%), hydrochloric acid (HCl, 35-37%), sodium hydroxide (NaOH, 98%), sodium chloride (NaCl, 99.5%), phenolphthalein ($C_{20}H_{14}O_4$, 98%), ethanol (C_2H_5OH, 99.5%), and methanol (CH_3OH, 99.9%) were supplied from Samchun Chemicals (Korea). Sodium carbonate (Na_2CO_3, 99.5%) and methyl yellow (indicator, 98%) were obtained from Kanto Chemical and Tokyo Chemical, respectively.

2. Catalyst Preparation

D-Glucose, the precursor of carbon supports, was dried and thoroughly ground before carbonization. Carbonization of glucose was carried out at different temperatures ranging from 573 to 973 K under nitrogen (100 mL/min) for 10 h. The resulting partially pyrolyzed GCx samples were denoted as GCx (x=1-5), depending on the carbonization temperature (Table 1).

Sulfonation involved contacting GCx with H_2SO_4 at an elevated temperature. For instance, 10 g of the GC2 sample was dispersed in 200 mL of H_2SO_4 (98%) in a three-necked flask (500 mL) connected to a condenser. After gentle stirring for 30 min to ensure homogeneous dispersion of the slurry, the temperature was raised to 453 K and sulfonation was conducted for 12 h under nitrogen. At the end of the sulfonation process, the slurry solution was cooled to an ambient temperature and then thoroughly washed with water until the pH of the filtrate remained constant. The resulting sulfonated GC2 (S-GC2) was dried at 383 K for 12 h and stored in a desiccator before use.

The Pd-supported GCx (Pd/GCx) catalysts were prepared by impregnation using a cationic Pd precursor. Typically, pre-determined $Pd(NH_3)_4(NO_3)_2$ solution (Pd intake 2 wt%) was slowly dropped on the dried GCx supports with thorough mixing. Aged at 298 K for 12 h, the Pd impregnated samples were dried at 393 K for 12 h and finally calcined at 523 K for 3 h under air (100 mL/min). The resulting catalysts were denoted as Pd/GCx (x=1-5). The Pd/S-GC2 catalyst was prepared in the same manner using the S-GC support. Pd/GC2R and Pd/S-GC2R were obtained by the reduction of Pd/GC2 and Pd/S-GC2 catalysts in the presence of mixed N_2/H_2 gas (1 : 1 v/v, 100 mL/min) at 473 K for 3 h, respectively.

3. Characterization

The concentration of surface functional groups on the GCx was determined by Boehm's chemical titration method [26,27]. Three basic reagents, such as NaOH, Na_2CO_3, and $NaHCO_3$, were used to neutralize the surface functionality of carbon materials based on their acid strength. For this purpose, carbon material (0.5 g) was treated with 0.01 N solution (20 mL) of each reagent for 24 h. After separating the carbon material, acid-base titration was performed to determine the base amount of the solution with phenolphthalein indicator. It is well known that while NaOH neutralizes all sulfonic acids, carboxylic acids, lactones, and phenols, Na_2CO_3 neutralizes carboxylic acids and lactones, and $NaHCO_3$ neutralizes carboxylic acids. Element Analysis (C, H, O, N, S) was carried out using a FlashSmart elemental analyzer (Thermo Fisher Scientific, USA).

X-ray diffraction (XRD) patterns of the prepared samples were analyzed using a Malvern Panalytical Empyrean high-resolution X-ray diffractometer. The binding energies of S and Pd were measured by X-ray photoelectron spectroscopy (XPS, Scientific MultiLab 2000, UK) with an Al anode at a pass energy of 50 eV, which was step incremented by 0.1 eV. A C 1s peak at 284.6 eV was considered as a reference to understand the other peak positions in the spectrum. Raman spectroscopy was performed using a high-resolution confocal Raman microscope (RAMANforce, Coax, Thailand) equipped with an ND filter 0.27% (100/255), an objective lens (TU Plan Flour 20x/NA 0.45), and a detector. Raman spectra were recorded using a 532.05 nm working laser (exposed for 9 s) and at a frequency range from 50 to 3,500 cm^{-1}. Diffuse reflectance infrared Fourier transform spectroscopy (DRIFTS) was performed using an FT-IR spectrometer (Nicolet iS50, Thermo Fisher Scientific, USA) with a diffuse reflectance chamber (Pike Technology). Spectra were recorded in the frequency range 400-4,000 cm^{-1} at a resolution of 32 cm^{-1} with 32 scans. Transmission electron microscopy (TEM) analysis was carried out using a JEOL 2100F (USA) instrument operating at 200 kV.

4. Direct Synthesis, Decomposition, and Hydrogenation Reaction of H_2O_2

The DSHP reaction was carried out under intrinsically safe reaction conditions in the absence of any caustic promoters, as described in our previous report [25]. Typically, the catalyst (20 mg) and mixed MeOH/H_2O solution (80 wt% MeOH) were poured into a 100 mL jacketed high-pressure reactor connected to a circulator; the temperature of the reaction solution was decreased to 275 K under nitrogen in a static mode. After eliminating any gaseous impurities, nitrogen was replaced with a mixture of two gases, such as 30 mL/min of H_2/N_2 (5 mol% H_2) and 10 mL/min of O_2/N_2 (20 mol% O_2). The pressure of the reactor was gradually increased up to 30 bar using two high-pressure mass flow controllers (MFCs) and maintained using a back pressure regulator (BPR) during the reaction. The reaction was performed for 1 h under vigorous stirring (1,200 rpm). During the reaction, off-gas was collected in a gas bag and the reaction product was separated from the catalyst by filtration for titration.

H_2 conversion was determined by gas chromatography analysis of the collected off-gas sample using an instrument (Agilent 6890N) equipped with a capillary column (Carboxen-1010 PLOT) and thermal conductivity detector. H_2O_2 concentration was determined by titrating the filtrate, obtained from the DSHP reaction, against a cerium sulfate ($Ce(SO_4)_2$) solution in the presence of ferroin as an indicator. H_2O_2 selectivity was calculated based on the determined H_2O_2 and H_2 concentrations. H_2O_2 productivity was defined as the amount of H_2O_2 produced per hour divided by the Pd content (mmol H_2O_2/g Pd h).

H_2O_2 decomposition and hydrogenation tests were conducted at 275 K under atmospheric pressure. For the H_2O_2 decomposition, the reaction solution consisted of 20 mg of catalyst and 50 g of mixed MeOH/H_2O solution containing 1 wt% H_2O_2 magnetically stirred for 1 h under nitrogen. H_2O_2 hydrogenation was carried out in a similar manner under bubbling H_2 (10 mL/min). During the H_2O_2 decomposition and hydrogenation tests, the liquid samples periodically extracted from the reactor were titrated to investigate the changes in the H_2O_2 concentration.

RESULTS AND DISCUSSION

1. Glucose-derived Amorphous Carbon

Glucose is the most abundant monosaccharide, with a molecular formula $C_6H_{12}O_6$. Usually, this natural product is not considered as a supporting material for the preparation of metal-supported catalysts because of its crystalline nature along with a very low surface area (<5 m^2/g). Despite its inadequacy as a supporting material, carbonization of glucose results in the formation of unique amorphous carbons structured as small and flexible polycyclic aromatic carbon sheets [28]. Moreover, the use of glucose-derived amorphous carbon as a supporting material offers the following advantages: i) it can be easily carbonized and converted to amorphous carbon with high reproducibility, ii) the oxygen-containing functional group content can be easily controlled by changing the carbonization temperature, and iii) a large number of sulfonic acid groups can be easily incorporated into the carbon structure.

In this study, a range of GCx (where x=1-5) was prepared by carbonization under different temperatures ranging from 573 to 973 K, as described in Scheme 2. Pyrolysis at relatively low temperatures resulted in the formation of incompletely carbonized carbon sheets with a three-dimensional *sp3*-bonded structure [29]. As the carbonization temperature increased, more rigid carbon networks were formed. Additional sulfonation was performed to incorporate the sulfonic acid group on the carbon surface by reacting GC2 with H_2SO_4 at an elevated temperature.

Table 1 shows the changes in the concentration of various functional groups on the GCx depending on the carbonization tempera-

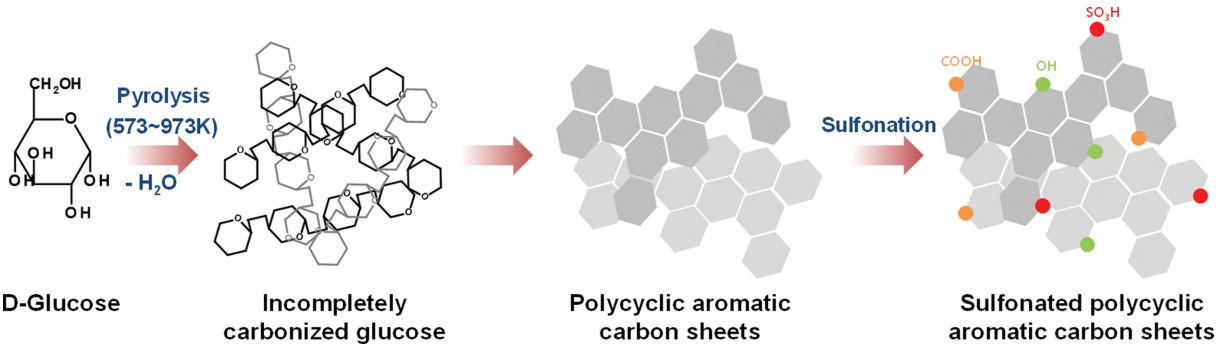

Scheme 2. Preparation of GCx and its sulfonation.

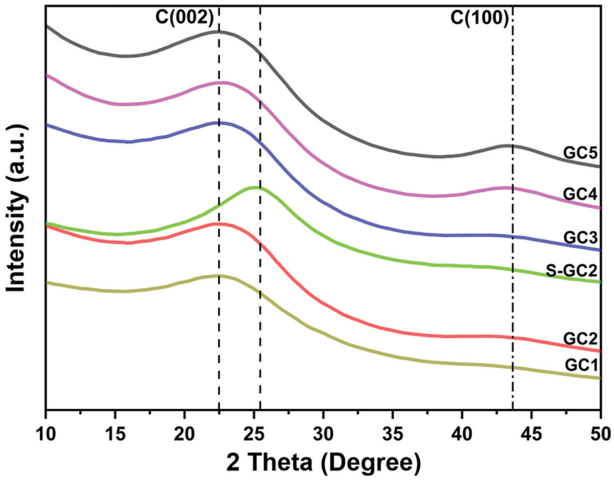

Fig. 1. Changes in the XRD patterns of GCx depending on the carbonization temperature and sulfonation.

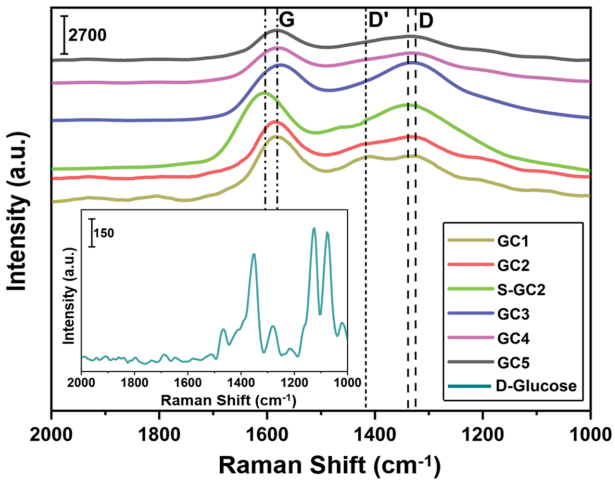

Fig. 2. Changes in the Raman spectra of GCx depending on the carbonization temperature and sulfonation. Inset shows the Raman spectrum of D-glucose.

ture and sulfonation. GC1 carbonized at a relatively low temperature (573 K) showed the highest total functional group concentration; the hydroxyl group content was approximately 80%, indicating that a small portion of glucose was pyrolyzed. It has been reported that carbonization below 523 K only results in complex polymeric materials composed of aromatic compounds [29]. As the carbonization temperature increased, not only the total functional group concentration but also their distribution was changed. In the cases of GC4 and GC5 carbonized above 873 K, the total functional group content was reduced to as low as *ca.* 40% of that of GC1; only the carbonyl group existed on the carbon surface. Sulfonation of GC2 significantly increased the functional group concentration on GC2. In particular, the sulfuric acid group was responsible for *ca.* 89% of the functional group concentration. The high sulfonation efficiency clearly showed that the unique flexible carbon sheet structure of the GCx could accommodate the high-density SO_3H groups [30]. In the case of carbon materials exhibiting electrical conductivity, only a limited amount of SO_3H groups can be incorporated [25,31].

Fig. 1 presents the XRD patterns of the GCx prepared by carbonization at different temperatures, followed by sulfonation. Regardless of the carbonization temperature, two broad diffraction peaks at approximately 20° and 45° were observed. These two peaks attributed to the graphitic C(002) and C(101) planes, respectively, indicate the existence of disordered polycyclic aromatic carbon sheets in the GCx structure [32,33]. The gradual increase in the peak intensities as a function of temperature might be ascribed to the stacking of carbon sheets. The C(002) peak shift in the S-GC2 pattern implied that smaller polycyclic carbon rings were formed during the sulfonation process, and therefore, the structural disorder of the GCx increased [34,35].

The Raman spectra of the GCx are shown in Fig. 2. In the case of D-glucose (inset), a number of sharp peaks were observed between 1,000 and 1,500 cm^{-1} due to the exo-/endo-cyclic C-O and C-C stretching or C-O-H deformations [36,37]. On the other hand, the distinct peaks of glucose completely disappeared after carbonization, and two representative peaks of amorphous carbon were clearly seen. The D (A1g symmetry) and G (E2g symmetry) bands appeared at ca. 1,320 and 1,580 cm^{-1}, which might be attributed to the defects of the amorphous carbon and *sp2* hybridized carbon network, respectively, indicating the existence of polycyclic aromatic carbon sheets in the GCx structure [17,38,39]. In the case of GC1, the weak D′ band *ca.* 1,420 cm^{-1} might be ascribed to the CH_2 or C-O-H bond of D-glucose [37,40], which suggests that considerable number of oxygen-containing groups still existed on GC1 carbonized under a relatively lower temperature. After sulfonation, the D and G bands of GC2 shifted slightly, implying that the polycyclic aromatic structure of GC2 was slightly changed by the sulfonation, as discussed in the XRD analysis.

2. Pd Catalysts Supported on the Glucose-derived Amorphous Carbons

A series of Pd/GCx (x=1-5) catalysts were prepared by the impregnation of a cationic Pd precursor on GCx or its sulfonated derivative. The XRD patterns of the Pd/GCx catalysts presented in Fig. 3(a) indicate that the peak intensities of various Pd crystal phases were affected by the carbonization temperature of GCx. Interestingly, the peak intensity of the Pd(111) phase for the Pd/GC2 catalyst was considerably lower than that for others, which implies that the Pd NP size was significantly different, as will be discussed later in the TEM analysis. Moreover, not only sulfonation of the GCx but also reduction exerted a significant impact on the crystallinity of Pd. As shown in Fig. 3(b), the peak intensity of both Pd(111) and Pd(200) phases was considerably increased after reduction. Conversely, only a broad and weak Pd(111) peak was observed in the amplified XRD patterns of both Pd/S-GC2 and Pd/S-GC2R. As presented in Table 2, the estimated Pd NP size according to the Scherrer equation based on the full width at half maximum of the Pd(111) phase indicates that sulfonation and reduction affected the Pd NP size of the Pd/GC2 series. However, the Pd NPs supported on S-GC2 were stable against sintering even under the reduction condition.

TEM images of the Pd/GCx catalysts and their Pd NP size distributions are presented in Fig. 4. As expected, the carbonization temperature of the GCx greatly affected the Pd NP size. There was

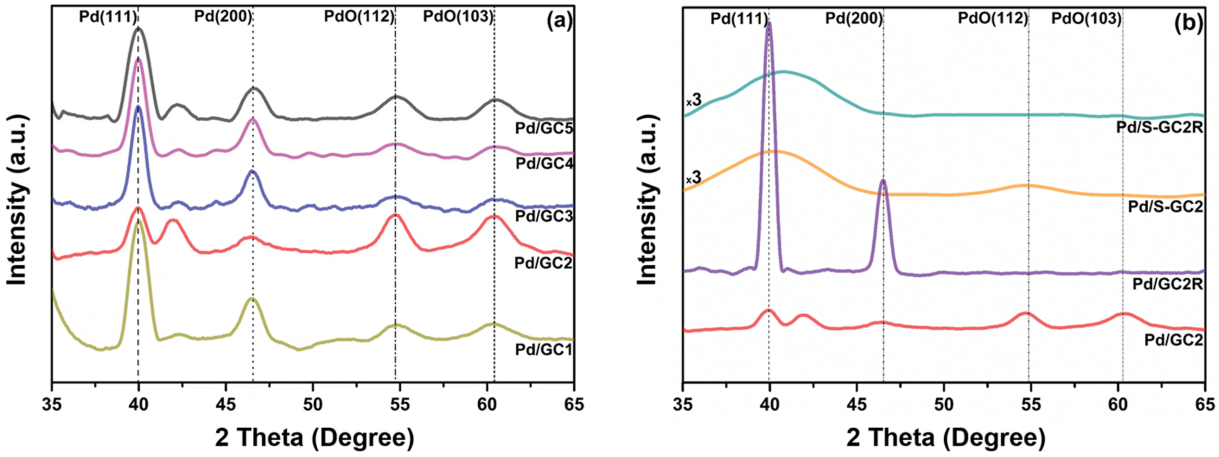

Fig. 3. Changes in the XRD patterns of Pd/GCx (x=1-5): (a) Depending on the carbonization temperature, and (b) depending on the reduction and sulfonation.

Table 2. Changes in the Pd NP size of the Pd/GC2 catalyst by reduction and sulfonation

Catalyst	Pd/GC2	Pd/GC2R	Pd/S-GC2	Pd/S-GC2R
Pd Nanoparticle size (nm)[a]	2.74	5.52	<2[b]	<2[b]

[a]Estimated by the Scherrer equation based on the full width at half maximum of the Pd(111) phase
[b]Below calculation limit

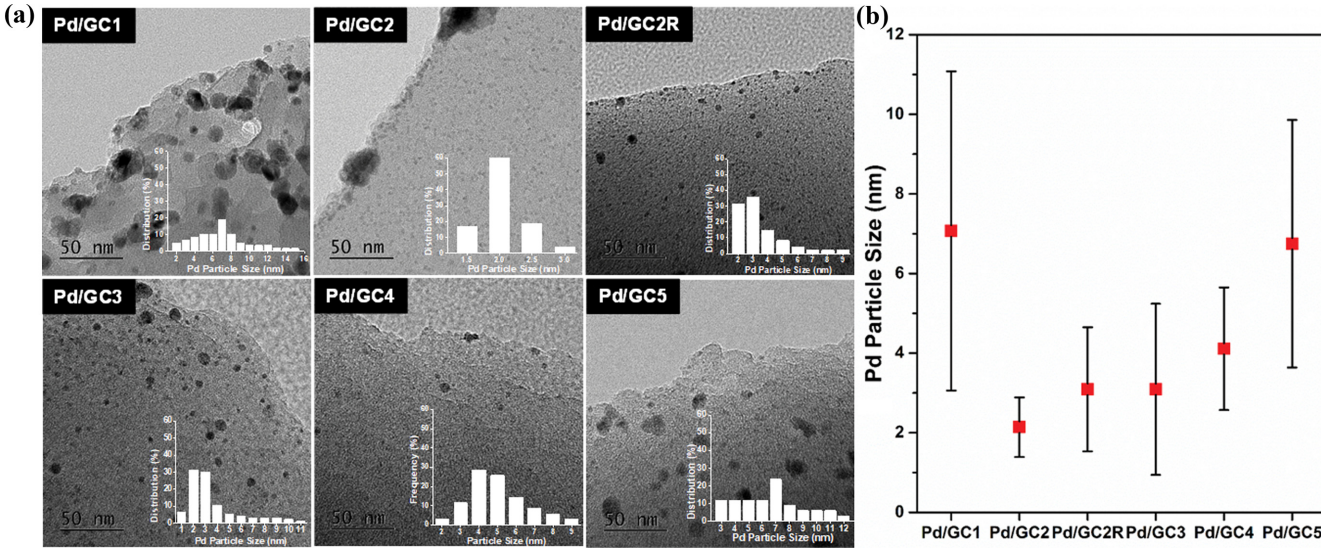

Fig. 4. (a) TEM images of Pd/GCx catalysts and (b) their Pd NP size distributions.

an obvious reverse volcano-shaped dependency of the Pd NP size on the carbonization temperature, and GC2 was favorable for the formation of very small and monodisperse Pd NPs. Although the largest number of oxygen-containing groups exists on the GC1 surface, the largest Pd NPs with the broadest size distribution were also formed on GC1. It seems that the oxygen groups on the incompletely carbonized GC1 surface were not efficient in suppressing the aggregation of Pd NPs during catalyst preparation. Conversely, in the cases of Pd/GC3, Pd/GC4, and Pd/GC5, the gradual increase in the Pd NP size might be ascribed to the reduced number of functional groups as the carbonization temperature increased. These results indicate that the surface property of the GCx altered by the carbonization temperature played a crucial role in determining the Pd NP size.

In addition to the carbonization temperature, the modified carbon surface by sulfonation might affect the Pd NP size. However, no appreciable Pd NPs were observed in the TEM images of Pd/S-GC2 and Pd/S-GC2R in spite of multiple TEM observations. As the existence of Pd was confirmed by other methods such as XRD, XPS, and EDS, it is assumed that very small Pd NPs were formed on the S-GC2 surface, as confirmed by the Pd NP size estimation shown in Table 2.

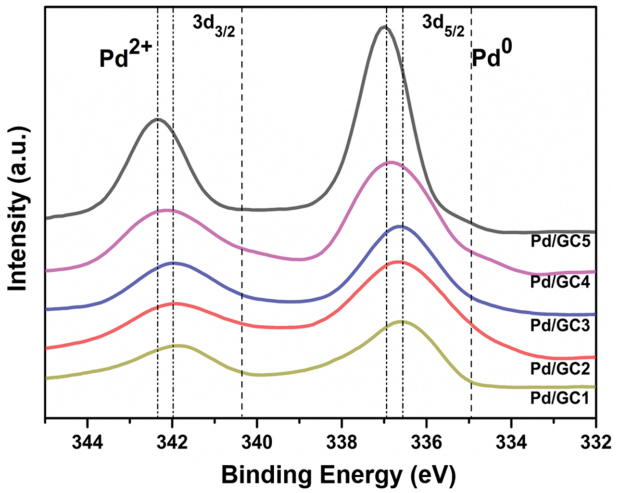

Fig. 5. Changes in the Pd 3d XPS spectra of Pd/GCx catalysts depending on the carbonization temperature.

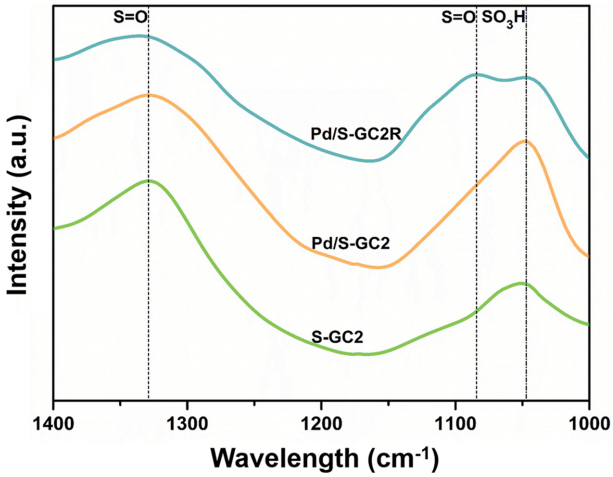

Fig. 7. DRIFTS scans of S-GC2, Pd/S-GC2, and Pd/S-GC2R.

XPS spectra of the Pd/GCx catalysts are shown in Fig. 5. The two strong peaks centered at approximately 336.5 and 342 eV could be ascribed to the Pd $3d_{5/2}$ and Pd $3d_{3/2}$ peaks of Pd^{2+}, respectively [41,42], indicating that most Pd existed in the oxidized form regardless of the carbonization temperature. The gradual shifts of both the Pd $3d_{5/2}$ and Pd $3d_{3/2}$ peaks of Pd^{2+} as a function of carbonization temperature imply that the interaction between Pd and the surface of GCx became weaker as the number of functional groups decreased [43,44].

Fig. 6 presents the XPS spectra of the Pd/GC2 series; they were analyzed to investigate the changes in the electronic state of Pd by sulfonation and reduction. As shown in Fig. 6(a), the Pd $3d_{5/2}$ and Pd $3d_{3/2}$ peaks of Pd/S-GC2 and Pd/S-GC2R were similar to those of Pd/GC2 and Pd/GC2R, respectively, implying that sulfonation did not affect the electronic property of Pd. Moreover, the Pd^{2+}/Pd^{0} ratio of Pd/S-GC2R was as low as that of Pd/GC2R, indicating that Pd could be easily reduced regardless of sulfonation (Fig. 6(b)).

The incorporation of sulfonic acid groups in GC2 was also confirmed by DRIFTS analysis. As shown in Fig. 7, the characteristic stretching bands of sulfonic acid groups were clearly observed in the DRIFTS scans of S-GC2, Pd/S-GC2, and Pd/S-GC2R. For example, the vibration band appearing around 1,050 cm^{-1} might be ascribed to the stretching of the -SO_3H group [45]. Another band at about 1,330 cm^{-1} and shoulder around 1,080 cm^{-1} could be assigned to the asymmetric and symmetric stretching of S=O bond, respectively [46,47].

The changes in the chemical states of sulfur during the impreg-

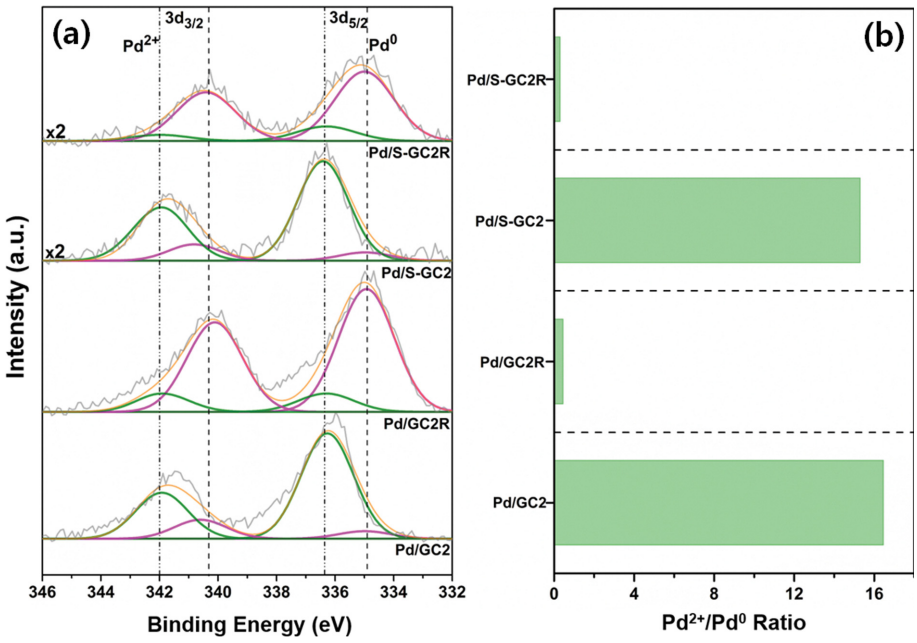

Fig. 6. (a) Changes in the Pd 3d XPS spectra of the Pd/CG2 series depending on sulfonation and reduction, and (b) changes in the Pd^{2+}/Pd^{0} ratio based on the deconvoluted Pd 3d XPS spectra.

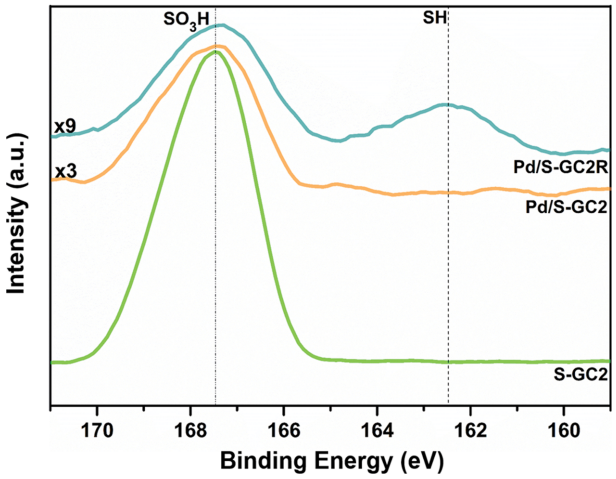

Fig. 8. Changes in the S 2p XPS spectra of S-GC2 series by Pd impregnation and reduction.

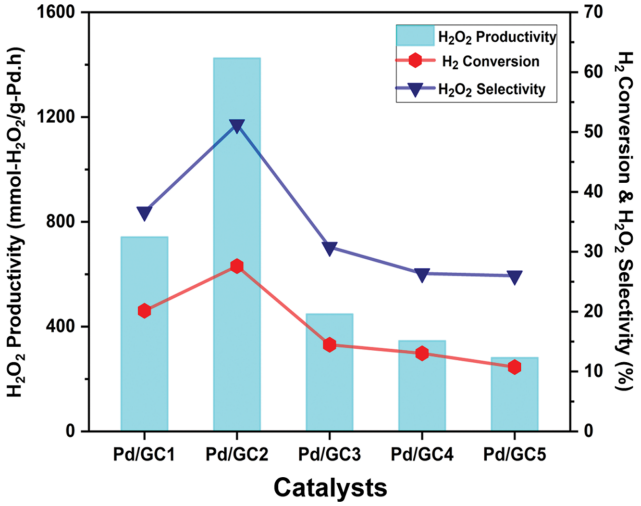

Fig. 10. DSHP in the presence of Pd/GCx catalysts.

nation of Pd and its subsequent reduction were investigated by S 2p XPS analysis, and the results are presented in Fig. 8. The strong peak at around 167.5 eV could be assigned to the S $2p_{3/2}$ peak of sulfonic acid [29,48], indicating successful incorporation of sulfonic acid groups on the GC2 surface. The reduced S $2p_{3/2}$ peak intensity of Pd/S-GC2 suggests that the concentration of surface sulfonic acid groups decreased during catalyst preparation. In the case of Pd/S-CG2R, the S $2p_{3/2}$ peak intensity decreased, accompanied by a broad peak centered at approximately 162.5 eV, which corresponded to the S $2p_{3/2}$ peak of the thiol (-SH) group [49]. The result implied that surface sulfonic acid groups were partially reduced to thiol groups during the reduction process.

Fig. 9 shows the changes in the pH of the reaction solution in the presence of Pd/GC2 and its sulfonated derivative. Pd impregnation and sequential reduction gradually increased the pH of the reaction solution regardless of sulfonation. However, the pH of the reaction solution decreased to *ca.* 3.8 in the presence of Pd/S-GC2, suggesting its promising potential as a solid acid support. After reduction (Pd/S-GC2R), the pH of the reaction solution was considerably increased due to the decrease in the number of sulfonic acid groups on the carbon surface during reduction, as examined in the S 2p XPS analysis.

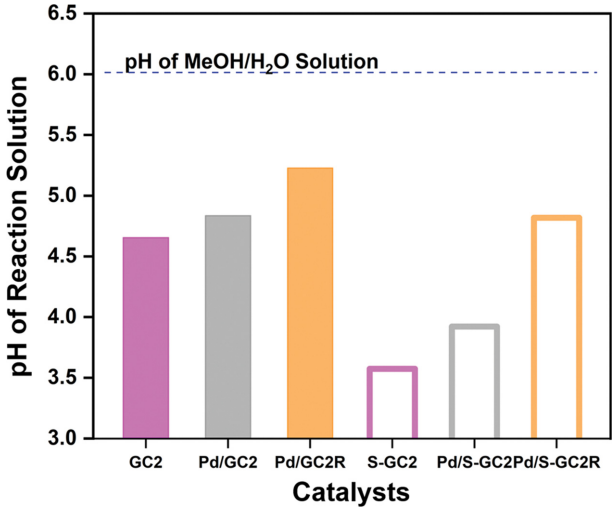

Fig. 9. Changes in the pH of reaction solution depending on the surface property of GC2 modified by sulfonation, Pd impregnation, and subsequent reduction.

3. Catalytic Activity for the Direct Synthesis of H_2O_2

The catalytic activity of Pd/GCx for the DSHP reaction was evaluated under intrinsically safe reaction conditions in the absence of any caustic additives. As shown in Fig. 10, there was an apparent volcano-shaped dependency of all reaction parameters, *i.e.*, H_2 conversion, H_2O_2 selectivity, and H_2O_2 productivity, on the carbonization temperature of GCx. Considering the reverse volcano-shaped relationship between the Pd NP size and the carbonization temperature of GCx, as observed in the TEM analysis, the smallest Pd NP size in the Pd/GC2 catalyst within the sub-nanometer domain was favorable in maximizing the catalytic performance [44].

Comparison of the catalytic performance of Pd/GC3 with that of Pd/GC4 and Pd/GC5 more clearly elucidated the crucial role of Pd NP size in promoting the DSHP reaction. Pd impregnation on the surface of GCx prepared at higher temperatures resulted in the formation of larger Pd NPs, resulting in reduced catalytic activity. In the case of Pd/GC1, while large and polydisperse Pd NPs were formed, its catalytic activity was better than that of Pd/GC3, Pd/GC4, and Pd/GC5. These results suggest that other factors, such as different surface functional group properties determined by the carbonization temperature, had a large impact on the catalytic activity as well as the Pd NP size.

Fig. 11 demonstrates that the catalytic performance of Pd/GCx for the DSHP reaction was also significantly affected by the use of sulfonated support and subsequent reduction. The improved H_2O_2 selectivity of the Pd/S-GC2 catalyst could be rationalized in terms of the beneficial role of the surface sulfonic acid groups, enabling S-GC2 to act as an efficient solid acid support. However, both H_2 conversion and H_2O_2 productivity were significantly decreased in the presence of the Pd/S-GC2 catalyst. According to density functional theory calculations, the Pd NP size has a huge impact on the

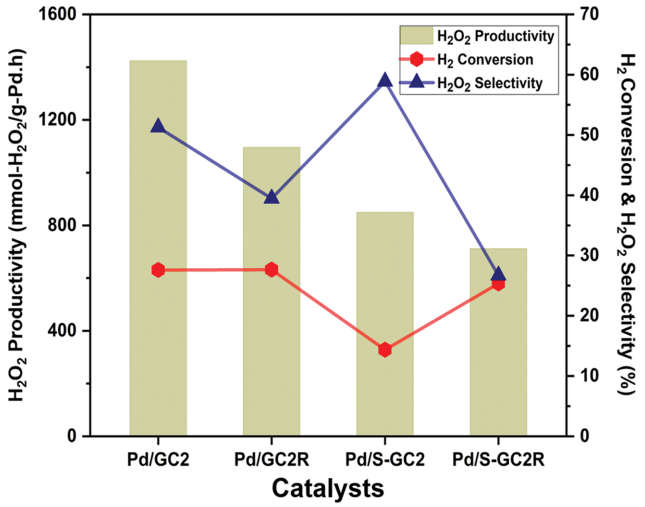

Fig. 11. Changes in the reaction performance of Pd/GC2 catalyst for DSHP by sulfonation and reduction.

catalytic performance of Pd. Pd nanoclusters within the sub-nanometer range (1.4-2.5 nm) offer more favorable active sites for selective oxygen hydrogenation than O-O dissociation. On the other hand, undesirable O-O dissociation may be accelerated on Pd NPs within the nanometer range (>2.5 nm). Very small Pd nanoclusters below the sub-nanometer range or single-site Pd do not promote the reaction because of the insufficient number of active sites [44].

The reduced H_2O_2 selectivity of both Pd/GC2R and Pd/S-GC2R catalysts might be ascribed either to the enhanced metallic nature or enlarged Pd NP size caused by reduction, as confirmed by the Pd 3d XPS or TEM analysis, respectively. In the case of the Pd/S-GC2R catalyst, partial loss of the sulfonic acid groups on the carbon surface during reduction might be additionally responsible for the sharp reduction in the H_2O_2 selectivity.

4. H_2O_2 Decomposition and Hydrogenation Tests

One of the inherent problems of the DSHP reaction is side reactions such as direct H_2 oxidation and subsequent decomposition and hydrogenation of H_2O_2 (Scheme 1). Therefore, not only the promotion of the DSHP reaction but also an efficient suppression of undesirable side reactions is of prime importance in terms of attaining a high H_2O_2 selectivity. In this regard, H_2O_2 decomposition and hydrogenation tests were carried out in the presence of Pd/GCx catalysts.

As shown in Fig. 12, the carbonization temperature of GCx also played an important role in determining the catalytic performance of Pd/GCx for H_2O_2 decomposition and hydrogenation. It was

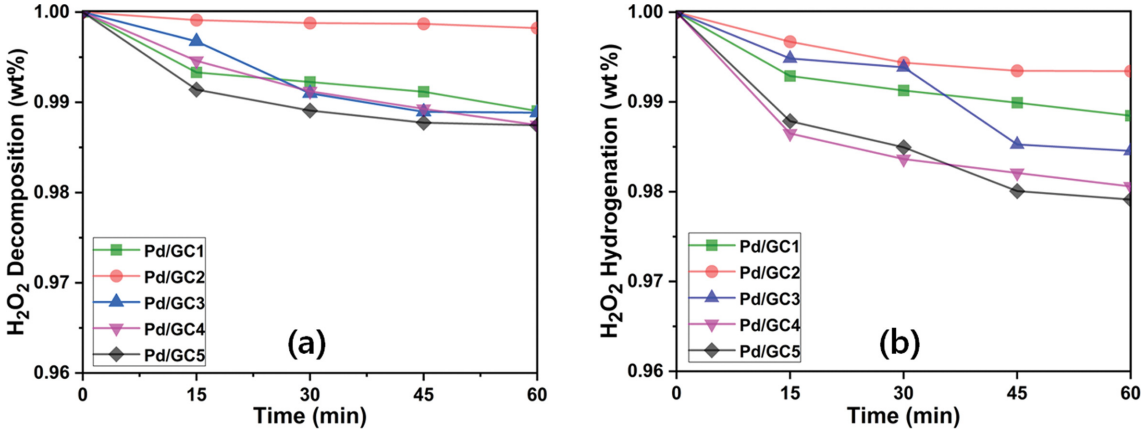

Fig. 12. (a) H_2O_2 decomposition and (b) H_2O_2 hydrogenation tests in the presence of Pd/GCx catalysts.

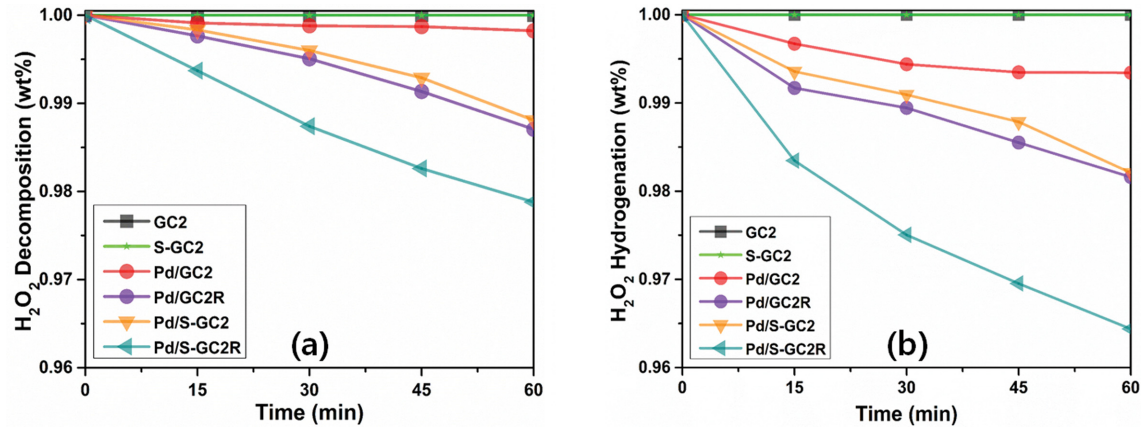

Fig. 13. Effect of sulfonation and reduction on the catalytic activity of Pd/GC2 for (a) H_2O_2 decomposition and (b) H_2O_2 hydrogenation.

revealed that the use of the Pd/GC2 catalyst containing sub-nanometer Pd NPs was favorable in suppressing the decomposition and hydrogenation of the produced H_2O_2. On the other hand, the higher H_2O_2 decomposition and hydrogenation rates observed in the presence of other Pd/GCx (where x=1, 3, 4, and 5) catalysts might be attributed to their larger Pd NP size. In particular, the different H_2O_2 hydrogenation rates with respect to the Pd/GCx catalysts (Fig. 12(b)) were well matched with the volcano-shaped dependency of the catalytic performance of the Pd/GCx catalysts on the carbonization temperature.

Fig. 13 presents the changes in the catalytic activity of Pd/GC2 for H_2O_2 decomposition and hydrogenation after sulfonation and reduction. The results obtained in the presence of GC2 or S-GC2 indicated that the unsupported GCx did not promote H_2O_2 decomposition and hydrogenation, regardless of sulfonation. However, it is interesting that H_2O_2 decomposition and hydrogenation proceeded faster over Pd/S-GC2 compared to over Pd/GC2. It seems that while the small Pd nanoclusters below the sub-nanometer size on Pd/S-GC2 were not effective in promoting the DSHP reaction, they preferentially catalyzed H_2O_2 hydrogenation. The significantly high H_2O_2 hydrogenation rate observed in the presence of Pd/S-GC2R implied that the reduced small Pd nanoclusters became more active in promoting H_2O_2 hydrogenation. These results demonstrate that fine-tuning of the physicochemical properties of Pd NPs by optimizing the carbonization temperature, followed by sulfonation and reduction, is important in designing an efficient Pd catalyst supported on GCx.

CONCLUSION

Pd catalysts supported on biomass-derived amorphous carbons were prepared, and their catalytic activity for the direct synthesis of hydrogen peroxide (DSHP) was investigated. D-glucose was pyrolyzed at different temperatures ranging from 573 to 973 K. The carbonization temperature exerted a crucial effect on the physicochemical properties of the glucose-derived carbons (GCx, where x=1-5) and consequently on the impregnated Pd NP size. It was revealed that the Pd/GC2 catalyst prepared at 723 K showed excellent catalytic performance, which might be ascribed to the formation of monodisperse Pd NPs within the sub-nanometer domain (1.4-2.5 nm). Although the Pd catalyst supported on the sulfonated derivative of the carbon substrate (Pd/S-GC2) was beneficial in improving the H_2O_2 selectivity, the clustered or single-site Pd was not efficient in increasing the reaction rate because of the insufficient number of active sites. The reduction of catalysts caused the formation of enlarged Pd NPs with a high metallic nature, which resulted in a decrease in H_2O_2 selectivity. These results clearly indicate that fine-tuning of the geometric and electronic nature of Pd NPs by optimizing the carbonization temperature, followed by sulfonation and reduction is a prerequisite for preparing Pd catalyst supported on the GCx for the DSHP reaction.

ACKNOWLEDGEMENT

This research was supported by Basic Science Research Program through the National Research Foundation of Korea (NRF) funded by the Ministry of Education (2016R1D1A3B02006928).

REFERENCES

1. G. Goor, J. Glenneberg and S. Jacobi, *Hydrogen Peroxide in Ullmann's Encycl. Ind. Chem*., Wiley-VCH Verlag GmbH, Weinheim (2012).
2. J. M. Campos-Martin, G. Blanco-Brieva and J. L. G. Fierro, *Angew. Chem. Int. Ed.*, **45**, 6962 (2006).
3. C. Samanta, *Appl. Catal. A Gen.*, **350**, 133 (2008).
4. S. Ranganathan and V. Sieber, *Catalysts*, **8**, 379 (2018).
5. F. Menegazzo, M. Signoretto, E. Ghedini, G. Strukul, F. Menegazzo, M. Signoretto, E. Ghedini and G. Strukul, *Catalysts*, **9**, 251 (2019).
6. J. S. J. Hargreaves, Y.-M. Chung, W. S. Ahn, T. Hisatomi, K. Domen, M. C. Kung and H. H. Kung, *Appl. Catal. A Gen.*, **594**, 117419 (2020).
7. S. Yang, A. Verdaguer-Casadevall, L. Arnarson, L. Silvioli, V. Colic, R. Frydendal, J. Rossmeisl, I. Chorkendorff and I. E. L. Stephens, *ACS Catal.*, **8**, 4064 (2018).
8. J. K. Edwards, S. J. Freakley, A. F. Carley, C. J. Kiely and G. J. Hutchings, *Acc. Chem. Res.*, **47**, 845 (2014).
9. D. W. Flaherty, *ACS Catal.*, **8**, 1520 (2018).
10. M. Seo, H. J. Kim, S. S. Han and K. Y. Lee, *Catal. Surv. from Asia*, **21**, 1 (2017).
11. R. J. Lewis and G. J. Hutchings, *ChemCatChem*, **11**, 298 (2019).
12. H.-U. Blaser, A. Indolese, A. Schnyder, H. Steiner and M. Studer, *J. Mol. Catal. A Chem.*, **173**, 3 (2001).
13. M. L. Toebes, J. A. Van Dillen and K. P. De Jong, *J. Mol. Catal. A Chem.*, **173**, 75 (2001).
14. X. Xiao, T. U. Kang, H. Nam, S. H. Bhang, S. Y. Lee, J. P. Ahn and T. Yu, *Korean J. Chem. Eng.*, **35**, 2379 (2018).
15. Y. Jang, H. Nam, J. Song and S. Lee, *Korean J. Chem. Eng.*, **36**, 1417 (2019).
16. J. K. Edwards, B. Solsona, E. Ntainjua, A. F. Carley, A. A. Herzing, C. J. Kiely and G. J. Hutchings, *Science*, **323**, 1037 (2009).
17. B. Hu, W. Deng, R. Li, Q. Zhang, Y. Wang, F. Delplanque-Janssens, D. Paul, F. Desmedt and P. Miquel, *J. Catal.*, **319**, 15 (2014).
18. T. García, S. Agouram, A. Dejoz, J. F. Sánchez-Royo, L. Torrente-Murciano and B. Solsona, *Catal. Today*, **248**, 48 (2015).
19. R. Arrigo, M. E. Schuster, S. Abate, G. Giorgianni, G. Centi, S. Perathoner, S. Wrabetz, V. Pfeifer, M. Antonietti and R. Schlögl, *ACS Catal.*, **6**, 6959 (2016).
20. S. Yook, H. C. Kwon, Y. G. Kim, W. Choi and M. Choi, *ACS Sustain. Chem. Eng.*, **5**, 1208, (2017).
21. S. Lee, H. Jeong and Y.-M. Chung, *J. Catal.*, **365**, 125 (2018).
22. S. Lee and Y.-M. Chung, *Mater. Lett.*, **234**, 58 (2019).
23. S. Lee and Y.-M. Chung, *Catal. Today*, **352**, 270 (2020).
24. V. T. T. Hang and Y.-M. Chung, *Korean J. Chem. Eng.*, **37**, 65 (2020).
25. H. T. T. Vu, V. L. N. Vo and Y.-M. Chung, *Appl. Catal. A Gen.*, **607**, 117867 (2020).
26. S. L. Goertzen, K. D. Thériault, A. M. Oickle, A. C. Tarasuk and H. A. Andreas, *Carbon*, **48**, 1252 (2010).
27. H. Jeon and Y.-M. Chung, *Appl. Catal. B Environ.*, **210**, 212 (2017).
28. M. Toda, A. Takagaki, M. Okamura, J. N. Kondo, S. Hayashi, K. Domen and M. Hara, *Nature*, **438**, 177 (2005).
29. K. Nakajima and M. Hara, *ACS Catal.*, **2**, 1296 (2012).

30. M. Hara, T. Yoshida, A. Takagaki, T. Takata, J. N. Kondo, S. Hayashi and K. Domen, *Angew. Chem. Int. Ed.*, **43**, 2955 (2004).
31. S. Suganuma, K. Nakajima, M. Kitano, S. Hayashi and M. Hara, *ChemSusChem*, **5**, 1841 (2012).
32. S. K. Mohamed, M. Abuelhamd, N. K. Allam, A. Shahat, M. Ramadan and H. M. A. Hassan, *Desalination*, **477**, 114278 (2020).
33. J. Wang, W. Xu, J. Ren, X. Liu, G. Lu and Y. Wang, *Green Chem.*, **13**, 2678 (2011).
34. K. Ngaosuwan, J. G. Goodwin and P. Prasertdham, *Renew. Energy*, **86**, 262 (2016).
35. W. W. Mar and E. Somsook, *Procedia Eng.*, **32**, 212 (2012).
36. G. Cerchiaro, A. C. Sant'Ana, M. L. A. Temperini and A. M. Da Costa Ferreira, *Carbohydr. Res.*, **340**, 2352 (2005).
37. A. F. Bell, L. D. Barron and L. Hecht, *Carbohydr. Res.*, **257**, 11 (1994).
38. H. He and C. Gao, *Molecules*, **15**, 4679 (2010).
39. X. Gu, W. Qi, X. Xu, Z. Sun, L. Zhang, W. Liu, X. Pan and D. Su, *Nanoscale*, **6**, 6609 (2014).
40. Y. Qu, A. Engdahl, S. Zhu, V. Vajda and N. McLoughlin, *Astrobiology*, **15**, 825 (2015).
41. J. Kim, Y.-M. Chung, S.-M. Kang, C.-H. Choi, B.-Y. Kim, Y.-T. Kwon, T. J. Kim, S.-H. Oh and C.-S. Lee, *ACS Catal.*, **2**, 1042 (2012).
42. Y.-M. Chung, Y.-T. Kwon, T. J. Kim, S.-H. Oh and C.-S. Lee, *Chem. Commun.*, **47**, 5705 (2011).
43. Z. Khan, N. F. Dummer and J. K. Edwards, *Philos. Trans. R. Soc. A Math. Phys. Eng. Sci.*, **376**, 20170058 (2018).
44. P. Tian, L. Ouyang, X. Xu, C. Ao, X. Xu, R. Si, X. Shen, M. Lin, J. Xu and Y. F. Han, *J. Catal.*, **349**, 30 (2017).
45. A. C. Zaman, *J. Mol. Liq.*, **249**, 892 (2018).
46. S. Suganuma, K. Nakajima, M. Kitano, D. Yamaguchi, H. Kato, S. Hayashi and M. Hara, *J. Am. Chem. Soc.*, **130**, 12787 (2008).
47. S. Suganuma, K. Nakajima, M. Kitano, H. Kato, A. Tamura, H. Kondo, S. Yanagawa, S. Hayashi and M. Hara, *Micropor. Mesopor. Mater.*, **143**, 443 (2011).
48. M. Okamura, A. Takagaki, M. Toda, J. N. Kondo, K. Domen, T. Tatsumi, M. Hara and S. Hayashi, *Chem. Mater.*, **18**, 3039 (2006).
49. C. Wang, Z. Guo, W. Shen, A. Zhang, Q. Xu, H. Liu and Y. Wang, *J. Mater. Chem. A*, **3**, 6064 (2015).